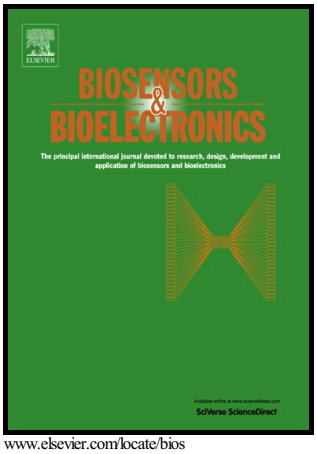

www.elsevier.com/locate/bios

Dual-mode electrochemical analysis of microRNA-21 using gold nanoparticle-decorated MoS_2 nanosheet

Shao Su, Wenfang Cao, Wei Liu, Zaiwei Lu, Dan Zhu, Jie Chao, Lixing Weng, Lihua Wang, Chunhai Fan, Lianhui Wang

PII: S0956-5663(17)30191-4
DOI: http://dx.doi.org/10.1016/j.bios.2017.03.040
Reference: BIOS9628

To appear in: *Biosensors and Bioelectronic*

Received date: 10 January 2017
Revised date: 16 March 2017
Accepted date: 18 March 2017

Cite this article as: Shao Su, Wenfang Cao, Wei Liu, Zaiwei Lu, Dan Zhu, Jie Chao, Lixing Weng, Lihua Wang, Chunhai Fan and Lianhui Wang, Dual-mode electrochemical analysis of microRNA-21 using gold nanoparticle-decorated MoS_2 nanosheet, *Biosensors and Bioelectronic* http://dx.doi.org/10.1016/j.bios.2017.03.040

Dual-mode electrochemical analysis of microRNA-21 using gold nanoparticle-decorated MoS_2 nanosheet

Shao Su,[1] Wenfang Cao,[1] Wei Liu,[1] Zaiwei Lu,[1] Dan Zhu,[1] Jie Chao,[1] Lixing Weng,[2] Lihua Wang,[3] Chunhai Fan[1, 3*], Lianhui Wang[1, *]

[1]Key Laboratory for Organic Electronics & Information Displays (KLOEID), Institute of Advanced Materials (IAM), National Syngerstic Innovation Center for Advanced Materials (SICAM), Nanjing University of Posts &Telecommunications, 9 Wenyuan Road, Nanjing 210023, China

[2]College of Geography and Biological Information, Nanjing University of Posts and Telecommunications, 9 Wenyuan Road, Nanjing, 210023, China

[3]Division of Physical Biology, Shanghai Institute of Applied Physics, Chinese Academy of Sciences, Shanghai 201800, China.

fanchunhai@sinap.ac.cn

iamlhwang@njupt.edu.cn.

Abstract

The detection of microRNA plays an important role in early cancer diagnosis. Herein, a dual-mode electronic biosensor was developed for microRNA-21 (miRNA-21) detection based on gold nanoparticle-decorated MoS_2 nanosheet (AuNPs@MoS_2). A classical DNA "sandwich" structure was employed to construct MoS_2-based electrochemical sensor, including capture DNA, target miRNA-21 and DNA-modified nanoprobe. $[Fe(CN)_6]^{3-/4-}$ and $[Ru(NH_3)_6]^{3+}$ were selected as electrochemical indicators to monitor the preparation process and evaluate the performance of MoS_2-based electrochemical biosensor by electrochemical impedance spectroscopy (EIS) and differential pulse voltammetry (DPV), respectively. Such MoS_2-based biosensor exhibited excellent performance for miRNA-21 detection in the range from 10 fM to 1 nM with detection limit of 0.78 fM and 0.45 fM for DPV and EIS technique, respectively. Furthermore, the proposed MoS_2-based biosensor displayed high selectivity and stability, which could be used to determine miRNA-21 in human serum samples with satisfactory results. All data suggested that such MoS_2-based nanocomposite may be a potential candidate for biosensing ranging from nucleic acid

to protein detection.

Keywords
dual-mode; molybdenum disulfide; gold nanoparticles; microRNA; biosensor

1 Introduction

MicroRNAs (miRNAs) are a class of short (about ~19-23 nucleotides) single-stranded noncoding RNAs, which can regulate gene expression (Dong et al., 2013; Cissell et al., 2007; Zhang et al., 2009). More and more evidences have proved that the expression of miRNAs are closely related with the occurrence, diagnosis, treatment and postoperative monitoring of cancer (Esquela-Kerscher et al., 2006; Sawyers, 2008; Li et al., 2014). Therefore, like protein, miRNAs have been considered as clinically important biomarkers for cancer early diagnosis. For example, miRNA-21 is found that it overexpressed in many cancers, such as lung adenocarcinomas, breast cancer, glioblastoma and so on (Lu et al., 2008; Medina and Slack, 2008). It should be noted that the expression level of miRNAs is relatively low and external environment easily make miRNA degrade. Therefore, it is highly demanded to develop accurate, rapid, sensitive, selective and low-cost methods for miRNAs detection.

Electrochemical technique has been considered as a promising method for sensitive and selective miRNA detection due to its advantages, such as rapid, simple, sensitive, low-cost and easy high-throughput (Drummond et al., 2003; Gao and Yang, 2006; Fan et al., 2007; Kilic et al., 2012; Chao and Fan, 2015). With the development of nanotechnology, nanomaterials have been extensively introduced into constructing electrochemical biosensors to improve the detection performance because of their large surface area, high electronic conductivity and high stability, such as DNA nanostructures (Lin et al., 2014; Pei et al., 2010), noble metal nanoparticles (Zhang et al., 2007), graphene (Cui et al., 2016), carbon nanotubes (Liu et al., 2015) and nanohybrids (Wu et al., 2014). It is well-known that different detection strategies combined with nanomaterials will generate different detection performance, including

label-free, labelled, classical DNA "sandwich" structure and kinds of amplification strategies. For example, noble metal nanostructures have been considered as ideal detection platforms for label-free and ultrasensitive miRNA detection (Yang et al., 2009; Su et al., 2016). Fan's group used DNA nanostructure as a sensing platform to sensitively and selectively determine miRNA in ideal and real samples. Such interesting sensing platform combined with enzyme-assisted amplification, which could detect as low as 10 aM miRNA-21 (Wen et al., 2012). Shuai et al. used graphene-based nanoprobe combined with sandwich-type DNA nanostructure as detection system, which could greatly improve detection signal with the enzymatic-assisted amplification (Shuai et al., 2017). The proposed biosensor exhibited a low detection limit of 50 aM for miRNA-21 detection. So many detection strategies combined with nanomaterials have been designed to sensitively and selectively detect miRNAs in ideal buffer and real samples. Unfortunately, most of those only chose single electrochemical signal mode to monitor the detection process and test the detection performance, such as electrochemical impedance spectroscopy (EIS), differential pulse voltammetry (DPV), square wave voltammetry (SWV) and so on (Cardoso et al., 2016; Cui et al., 2015; Jiang et al., 2014). As we know, EIS is usually used to monitor the electron transfer ability of the modified electrodes and detection process, while SWV and DPV often represent the peak currents of detection system. Therefore, different electrochemical method possessed different detection meaning. For comparison, it may be very interesting to use dual-mode for miRNAs detection in one detection strategy.

As we know, MoS_2 is a graphene-like layered nanomaterial, which is considered as promising sensing platform for chemical/biological molecules detection combined with fluorescence, electrochemistry, surface-enhanced Raman spectroscopy (SERS) and field-effect transistor (FET) techniques (Zhu et al., 2013; Li et al., 2016; Tian et al., 2015). MoS_2 has an interesting indirect-to-direct bandgap transition with the thickness of MoS_2 from bulk to single-layer, making it as a potential nanomaterial for constructing electrochemical sensors (Eda et al., 2011; Radisavljevic et al., 2011). It had been proved that MoS_2 nanosheet was a promising supporting material to

decorate noble metal nanoparticles (such as Au, Ag, Pt and Pd nanoparticles) (Huang et al., 2013), graphene (Chang and Chen, 2011) and other organic compounds (Bertolazzi et al., 2013), which could greatly enlarge its electrochemical application due to the synergistic effect. For example, Li's group proposed a MoS_2-based electrochemical biosensor for the detection of H_2O_2 and DNA with excellent detection performance, respectively (Wang et al., 2013; Wang et al., 2014). Wang et al. utilized the catalytical activity of MoS_2-Au nanocomposite to construct a sandwich-type immunosensor for carcinoembryonic antigen (CEA) detection, which could detect as low as 0.27 pg/mL CEA (Wang et al., 2015). Huang's group fabricated an electrochemical biosensor for highly sensitive detection of circulating tumor DNA based on the thin-layer MoS_2/graphene nanocomposites (Chu et al., 2016). Our group also had successfully used AuNPs-MoS_2 as an electrochemical sensing platform to detect chemical/biological molecules, including neurotransmitters, H_2O_2, ATP, thrombin and protein (Su et al., 2013; Chao et al., 2015; Su et al., 2016; Su et al., 2015). Herein, we reported a simple and sensitive dual-mode electrochemical platform for miRNA-21 detection using gold nanoparticles-decorated MoS_2 nanocomposites (AuNPs@MoS_2) as both electrode modifier and nanoamplifier. Such dual-mode electrochemical biosensing strategy combined with the advantages of AuNPs@MoS_2 nanocomposites and classical DNA "sandwich" structure. As shown in Scheme 1, thiolated DNA1 was immobilized on the surface of AuNPs@MoS_2 film modified electrode, which used to capture the target miRNA-21. Probe DNA2 was conjugated on the surface of AuNPs@MoS_2 nanocomposie as a nanoamplifier. As mentioned, there were many AuNPs supported on the surface of MoS_2 nanosheet, which could load large numbers of DNA2 probe. In our detection strategy, more DNA probe results in higher sensitivity. If no addition of target miRNA-21, only DNA1 strand immobilized on the surface of AuNPs@MoS_2/GCE, resulting in low electrochemical signals by using $[Fe(CN)_6]^{3-/4-}$ and $[Ru(NH_3)_6]^{3+}$ as electrochemical indicators (both EIS and DPV signals). A classical "sandwich" structure was formed in the presence of miRNA-21, making the EIS and DVP signals increased, respectively. As noted, both EIS and DPV signals were increased with the

concentration of miRNA-21 increasing. It should be pointed out that the increment of EIS signal was larger than DPV signal. The reason was ascribed to the layered structure of MoS_2-based nanocomposites, which hindered the electron transfer between redox probes and electrode when they immobilized on the surface of electrode during the formation of "sandwich" structure. Such detection strategy not only worked well in buffer, but also could determine miRNA-21 in serum with satisfactory results, suggesting that MoS_2-based nanocomposites maybe potential nanomaterials for biosensing.

2 Experimental Section

2.1 Reagents

Molybdenum (IV) sulfide powder (< 2 μm, 99%), gold (III) tetrachloride trihydrate ($HAuCl_4 \cdot 3H_2O$, ≥99%), 6-mercapto-1-hexanol (MCH, 97%) and hexaammineruthenium (III) chloride ($[Ru(NH_3)_6]Cl_3$, 98%) were purchased from Sigma-Aldrich (USA). Potassium hexacyanoferrate (III) ($K_3Fe(CN)_6$, ≥99.5%), potassium hexacyanoferrate (II) trihydrate ($K_4Fe(CN)_6 \cdot 3H_2O$, ≥99.5%), disodium hydrogen phosphate (Na_2HPO_4, ≥99.0%), sodium dihydrogen phosphate dehydrate ($NaH_2PO_4 \cdot 2H_2O$, ≥99.0%), ascorbic acid (AA, ≥99.7%), tris (hydroxymethyl) aminomethane (Tris, 99.0%), sodium chloride (NaCl, ≥99.5%), potassium chloride (KCl, ≥99.5%) and magnesium chloride hexahydrate ($MgCl_2$, ≥98%) were purchased from Sinopharm Chemical Reagent Co., Ltd (Shanghai, China). Polyvinyl pyrrolidone (PVP) was purchased from Alfa Aesar (Tianjin, China). Potassium nitrate (KNO_3, 99%) was purchased from Aladdin Industrial Corporation (Shanghai, China).

All chemicals were directly used without further purification. All solutions were prepared with Milli-Q water from a Milli-pore system.

The DNA and miRNA sequences used in the study were purchased from TaKaRa (Dalian, China), which were listed as follows:

DNA1: 5'-(SHC_6)TTTTTTCAACATCAG-3'

DNA2: 5'-TCTGATAAGCTATTTTT(SH)-3'

microRNA-21: 5'-UAGCUUAUCAGACUGAUGUUGA-3'

single-base mismatch RNA: 5'-UAGCUUAUCAGACUGAUGUUGC-3'

non-complementary RNA: 5'-UCCUGUACUGAGCUGCCCCGAG-3'

The buffer solutions used in this work were listed as follows: DNA immobilization buffer: 10 mM Tris–HCl, 5 mM $MgCl_2$ and 140 mM NaCl (pH 7.4). Electrochemical detection buffer for DPV: 10 mM Tris–HCl buffer (pH 7.4) containing 100 mM $[Ru(NH_3)_6]^{3+}$ and 100 mM KNO_3. Washing buffer: 10 mM Tris–HCl (pH 7.4). Electrochemical detection buffer for EIS: 10 mM Tris–HCl (pH 7.4) containing 5 mM $K_3[Fe(CN)_6]$, 5 mM $K_4[Fe(CN)_6]$ and 0.1 M KCl.

2.2 Apparatus

All electrochemical experiments were performed on Autolab PGSTAT302 (Metrohm China Ltd, Switzerland). A conventional three-electrode system was used in this experiment. Different modified glassy carbon electrodes (GCE) (3.0 mm in diameter) was used as working electrodes; a platinum wire and a saturated calomel electrode (SCE) were used as the auxiliary electrode and the reference electrode, respectively. The morphology of the MoS_2 nanosheet and the AuNPs@MoS_2 nanocomposite was observed using a transmission electron microscope (TEM, Philips CM 200). Automic force microscope (AFM, Bruker) was employed to examine the height of MoS_2 nanosheet. UV-vis-NIR-Spectrophotometer (UV-3600, Shimadzu) and Zeta Potential Analyzer (Zeta PALS, Brookhaven) were used to prove the conjugation of the DNA2 and AuNPs@MoS_2.

2.3 Preparation of AuNPs@MoS_2 and DNA2-AuNPs@MoS_2

MoS_2 nanosheet and AuNPs@MoS_2 were all prepared by our previous works (Su et al., 2014; Su et al., 2016). The conjugation of the DNA2 and AuNPs@MoS_2 (DNA2-AuNPs@MoS_2) was performed according to the literature (Tang et al., 2011). First, AuNPs@MoS_2 was purified for twice and diluted in 0.01 M pH 7.4 PBS finally to form AuNPs@MoS_2 suspension. Second, DNA2 solution (20 μL, 10 μM) was added to 180 μL of the as-prepared AuNPs@MoS_2 suspension containing 0.1 M NaCl. Then, the DNA2 and AuNPs@MoS_2 mixture was incubated overnight with slightly shaking at a constant temperature (25 ºC). Finally, the product was purified twice by centrifugation (5000 rpm, 30 min) to remove the free DNA2 and re-dispersed in 200

μL of 0.01 M pH 7.4 PBS.

2.4 Preparation of the sensor

A GCE was firstly mechanically polished with 0.3 mm and 0.05 mm alumina slurry, respectively. Then, the GCE was sonicated in ethanol and ultrapure water for several minutes, respectively. After drying under a nitrogen stream, 5 μL as-prepared AuNPs@MoS_2 solution was dropped onto the cleaned GCE and dried at the room temperature to constitute AuNPs@MoS_2/GCE. At first, 5 μL DNA1 (10 μM) was cast on the surface of the AuNPs@MoS_2/GCE for 16 h at room temperature to assemble the DNA1 on the electrode surface. After unbound DNA1 was removed by Tris–HCl buffer, the unreacted active sites were subsequently passivated with 5 μL 10 mM MCH solution at 37 °C for 1 h. Then the electrode was incubated with different concentrations of miRNA-21 and as-prepared DNA2-AuNPs@MoS_2 to obtain the DNA2-AuNPs@MoS_2/miRNA-21/MCH/DNA1/AuNPs@MoS_2/GCE.

3 Results and discussion

3.1 Characterization of MoS_2 nanosheet and AuNPs-MoS_2 nanocomposite

The morphologies of MoS_2 nanosheet and AuNPs@MoS_2 nanocomposite were characterized by TEM and AFM. As shown in Figure 1A, a thin layer of MoS_2 nanosheet was obtained with a typical crumpled and wrinkled structure. The thickness of the exfoliated MoS_2 nanosheet was measured by AFM. The average height of MoS_2 nanosheet was about 1.2 nm, indicating that the exfoliated MoS_2 nanosheet was almost single layer (Figure S1). With the addition of $HAuCl_4$, the AuNPs were in situ grown on the surface of MoS_2 nanosheet with an average diameter of 21 nm, suggesting AuNPs@MoS_2 nanocomposite had been successfully synthesized (Figure 1B).

3.3 Characterization of DNA2-AuNPs@MoS_2

It’s well-known that DNA molecules easily conjugate with AuNPs via the famous Au-S bond (Thavanathan et al., 2014). Herein, UV-vis absorption spectroscopy and Zeta potential analysis were used to characterize the conjugation of capture DNA2 and AuNPs@MoS_2 nanocomposite. Unfortunately, the UV-vis absorption peaks of DNA2-AuNPs@MoS_2 nanoconjugation and AuNPs@MoS_2

nanocomposite were overlapped because MoS_2 nanosheet had two absorption peaks at 253 nm and 262 nm (Figure S2). As shown in Figure S3, the potential of DNA2-AuNPs@MoS_2 nanoconjugation shifted to -40 mV, exhibiting an obvious negative shift compared with AuNPs@MoS_2 nanocomposite. As we know, DNA sequence generally possesses negative charge. Therefore, experimental data proved that the designed DNA2-AuNPs@MoS_2 nanoprobe had been successfully constructed.

3.4 Electrochemical characterization of the MoS_2-based biosensor

The feasibility of the dual-mode strategy for miRNA-21 detection was first investigated by cyclic voltammetry (CV) and EIS. As shown in Figure 2A, AuNPs@MoS_2 modified electrode showed a low signal because a few of $[Ru(NH_3)_6]^{3+}$ molecules was adsorbed on the surface of AuNPs@MoS_2/GCE (curve a). When capture DNA1 was immobilized on the surface of AuNPs@MoS_2/GCE, a large portion of $[Ru(NH_3)_6]^{3+}$ was bound to anionic phosphate of DNA strands, resulting in the electrochemical signal increased (curve b). Almost no change was obtained when MCH blocked the remaining active spots (curve c). It should be pointed out that the electrochemical signal was little change in the presence of nanoamplifier, suggesting that almost no non-specific adsorption existed (curve d). A pair of larger peaks was observed (curve e) in the presence of target miRNA-21 than that in the absence of miRNA-21 (curve d), indicating that DNA "sandwich" structure was successfully formed (Zhang et al., 2008). As we know, electrochemical impedance spectroscopy (EIS) was a powerful tool to monitor the electrode fabrication and electrochemical reaction process. Therefore, another electrochemical indicator ($[Fe(CN)_6]^{3-/4-}$) was employed to monitor this process of the MoS_2-based biosensor. The semicircle diameter of EIS was used to reflect the electron transfer resistance (R_{ct}). As shown in Figure 2B, the MoS_2/GCE (curve b) showed a larger semicircle diameter than that at bare GCE (curve a), implying MoS_2 nanosheet was successfully immobilized on the electrode surface. A large amount of negative charge on the surface of MoS_2 nanosheet and poor conductivity of MoS_2 nanosheet greatly hindered the electron transfer between $[Fe(CN)_6]^{3-/4-}$ and electrode, resulting in larger semicircle diameter.

The semicircle diameter of AuNPs@MoS_2/GCE (curve c) was smaller than that of MoS_2/GCE, indicating that AuNPs@MoS_2 possessed excellent conductivity and could greatly facilitate the electron transfer. If capture DNA1 was immobilized on the surface of AuNPs@MoS_2/GCE, the semicircle diameter obviously increased because DNA strand often possesses negative charges (curve d). Similar to probe $[Ru(NH_3)_6]^{3+}$, the semicircle diameters of MCH/DNA1/AuNPs@MoS_2/GCE (curve e) and DNA2-AuNPs@MoS_2/MCH/DNA1/AuNPs@MoS_2/GCE (curve f) were equal to or a little larger than that of DNA1/AuNPs@MoS_2/GCE, suggesting the remaining active spots was blocked and few non-specific adsorption existed. An obvious larger semicircle diameter was observed at DNA2-AuNPs@MoS_2/miRNA-21/MCH/DNA1/AuNPs@MoS_2/GCE (curve g) in the presence of miRNA-21, indicating that DNA "sandwich" structure formed. The corresponding cyclic voltammograms of different MoS_2-based electrodes were also proved the detection strategy worked (Figure S4). All the results proved that the designed strategy could be used to determine miRNA-21 by using two different signal modes.

3.5 Analytical performance of the MoS_2-based biosensor

The analytical performance of the MoS_2-based biosensor was evaluated by both DPV and EIS measurements. As shown in Figure 3A and Figure 3C, the peak currents and R_{ct} values of the MoS_2-based biosensor increased with miRNA-21 concentration increasing by using $[Ru(NH_3)_6]^{3+}$ and $[Fe(CN)_6]^{3-/4-}$ as electrochemical indicators, respectively. The variations ($\Delta I = I_{miRNA\text{-}21} - I_{no\ miRNA\text{-}21}$) in peak current of the biosensor was proportional to the logarithm value of miRNA-21 concentration in the range of 10 fM to 1 nM (Figure 3B). The linear regression equation can be presented as ΔI (μA) = 0.29 logc (fM) + 0.44 (R^2=0.98) and the detection limit was calculated to be 0.78 fM (S/N=3). Similarly, the ΔR_{ct} ($\Delta R_{ct} = R_{ct,\ miRNA\text{-}21} - R_{ct,\ no\ miRNA\text{-}21}$) was linear with the the logarithm value of miRNA-21 concentration ranging from 10 fM to 1 nM (ΔR_{ct} = 304.17 logc (fM) - 0.13, R^2=0.99) with detection limit of 0.45 fM (Figure 3D). Such linear range and detection limit of the MoS_2-based biosensor were comparable to or better than some published nanomaterials-based biosensors for microRNA detection

(Table S1).

3.6 Amplified effect of AuNPs@MoS_2-based nanoprobe

To investigate the amplified effects of AuNPs@MoS_2-based nanoprobe, a control electrode defined as DNA2/miRNA-21/MCH/DNA1/AuNPs@MoS_2/GCE was fabricated. As shown in Figure 4A and 4B, the current variation of DNA2-AuNPs@MoS_2/miRNA-21/MCH/DNA1/AuNPs@MoS_2/GCE was 1.66 folds than that of DNA2/miRNA-21/MCH/DNA1/AuNPs@MoS_2/GCE under the same condition, suggesting that the nanoamplifier could efficiently amplify the detection performance. It should be noted that the amplified effect of DNA2-AuNPs@MoS_2/miRNA-21/MCH/DNA1/AuNPs@MoS_2/GCE was different by using different electrochemical indicators. Obviously, the use of $[Fe(CN)_6]^{3-/4-}$ (2.13 folds) showed better amplified effect than that of $[Ru(NH_3)_6]^{3+}$ (1.66 folds) in the presence of 1 nM miRNA-21. The reason may be ascribed to the properties of AuNPs@MoS_2 nanocomposites. As mentioned above, AuNPs@MoS_2 nanocomposite was typical layered nanostructure with large surface area. When AuNPs@MoS_2-based nanoamplifer was assembled on the surface of the modified electrode, it could increase the amount of DNA stands and the thick of the modified electrode. As we know, the more DNA strands resulted in larger electrochemical signal by using $[Ru(NH_3)_6]^{3+}$ as redox probe. However, the thicker of the modified electrode leaded to poorer electrochemical signal under the same condition. Therefore, the final amplified effect was lower than as-expected. In contrast, the EIS technique monitored the electron transfer between redox probe and the modified electrode. The thicker of the modified electrode didn't influence the amplified effect, resulting in the amplified effect better than our expected. Therefore, if using layered nanomaterials as nanoamplifer, EIS technique may be an ideal choice. The detailed comparison of detection performances of DNA2/miRNA-21/MCH/DNA1/AuNPs@MoS_2/GCE and DNA2-AuNPs@MoS_2/miRNA-21/MCH/DNA1/AuNPs@MoS_2/GCE was shown in Figure S5, further proving the designed strategy worked well.

3.7 Selectivity of miRNA-21 biosensor

The selectivity of this MoS_2-based biosensor was investigated by adding the same concentrations (100 pM) of target miRNA-21, single-base mismatch miRNA-21 (SM-miRNA-21) and non-complementary miRNA (miRNA-486) into the detection system, respectively. As shown in Figure 5A, the ΔI of MoS_2-based biosensor was almost 2.0 μA in the presence of target miRNA-21, which was almost 4.32 folds and 16.41 folds than the addition of SM-miRNA-21 and miRNA-486, respectively. This result demonstrated that MoS_2-based biosensor showed an excellent selectivity toward target miRNA-21. The similar result was obtained by using EIS technique (Figure 5B), the ΔR_{ct} of MoS_2-based biosensor was almost 1442 Ω in the presence of target miRNA-21, which was almost 2.77 folds and 12.88 folds than the addition of SM-miRNA-21 and miRNA-486, respectively. All experimental data suggested that the as-prepared biosensor had a high selectivity for the determination of miRNA-21, which could efficiently distinguished target miRNA from one-base mismatch miRNA.

3.8 Real samples analysis

To evaluate the practicability of this biosensor, we simulated real detection system by adding miRNA-21 into human serum samples. The detection performance were listed in Table S2, which analyzed by DPV and EIS measurement, respectively. It could be noted that the rate of recovery was ranging from 90.16% to 102.90% and the relative standard deviation (RSD) was below 5%, suggesting such MoS_2-based biosensor possessed an acceptable detection performance.

4 Conclusions

In a word, a dual-mode detection strategy was developed based on AuNPs@MoS_2 nanocomposite. AuNPs@MoS_2 nanocomposite was not only used as an electrode modifier to immobilize capture DNA, but also used as a nanoprobe to amplify the detection performance. Two different electrochemical indicators were employed to monitor the preparation process and detection performance of MoS_2-based biosensor by DPV and EIS measurements, respectively. All experimental data showed such MoS_2-based biosensor possessed excellent sensitivity and

selectivity in ideal buffer and real samples, suggesting this MoS_2-based biosensor had a great potential for application in DNA/miRNA-related clinical diagnostics and biochemical research.

Acknowledgements

This work was financially supported by the National Natural Science Foundation of China (61671250, 21475064 and 21305070), the Sci-tech Support Plan of Jiangsu Province (BE2014719), the Program for Changjiang Scholars and Innovative Research Team in University (IRT_15R37), and the Priority Academic Program Development of Jiangsu Higher Education Institutions (PAPD, YX03002).

References:

Bertolazzi, S., Krasnozhon, D., Kis, A, 2013. ACS Nano. 7, 3246-3252.

Cardoso, A. R., Moreira, F. T., Fernandes, R., Sales, M. G., 2016. Biosens. Bioelectron. 80, 621-630.

Chang, K., Chen, W. X., 2011. ACS Nano. 5, 4720-4728.

Chao, J., Fan, C. H., 2015. Sci. China. Chem. 58, 834-834.

Chao, J., Zou, M., Zhang, C., Sun, H. F., Pan, D., Pei, H., Su, S., Yuwen, L. H., Fan, C. H., Wang, L. H., 2015. Nanotechnology. 26, 274005.

Chu, Y. L., Cai, B., Ma, Y., Zhao, M. G., Ye, Z. Z., Huang, J. Y., 2016. RSC. Adv. 6, 22673-22678.

Cissell, K. A., Shrestha, S., Deo, S. K., 2007. Anal. Chem. 79, 4754-4761.

Cui, H. F., Xu, T. B., Sun, Y. L., Zhou, A. W., Cui, Y. H., Liu, W., Luong, J. H. 2015. Anal. Chem. 87, 1358-1365.

Cui, X. H., Chen, H. Y., Yang, T., 2016. Acta. Chim. Sinica. 74, 392-400.

Dong, H. F., Lei, J. P., Ding, L., Wen, Y. Q., Ju, H. X., Zhang, X.J., 2013. Chem. Rev. 113, 6207-6233.

Drummond, T. G., Hill, M. G., Barton, J. K., 2003. Nat. Biotechnol. 21, 1192-1199.

Eda, G., Yamaguchi, H., Voiry, D., Fujita, T., Chen, M. W., Chhowalla, M., 2011. Nano Lett. 11, 5111-5116.

Esquela-Kerscher, A., Slack, F. J., 2006. Nat. Rev. Cancer. 6, 259-269.

Fan, Y., Chen, X. T., Trigg, A. D., Tung, C. H., Kong, J., Gao, Z. Q. J., 2007. Am. Chem. Soc. 129, 5437-5443.

Gao, Z. Q.; Yang, Z. C. Anal. Chem. 2006, 78, 1470-1477.

Huang, X.; Zeng, Z. Y.; Bao, S. Y.; Wang, M. F.; Qi, X. Y.; Fan, Z. X.; Zhang, H. Nat. Commun. 2013, 4, 1444.

Jiang, L., Qian, J., Yang, X. W., Yan, Y. T., Liu, Q., Wang, K., Wang, K., 2014. Anal. Chim. Acta.

806, 128-135.

Kilic, T., Topkaya, S. N., Ozkan Ariksoysal, D., Ozsoz, M., Ballar, P., Erac, Y., Gozen, O., 2012. Biosens. Bioelectron. 38, 195-201.

Li, X., Shan, J. Y., Zhang, W. Z., Su, S., Yuwen, L. H., Wang, L. H., 2016. Small. DOI: 10.1002/smll.201602660.

Li, J. B., Tan, S. B., Kooger, R., Zhang, C. Y., Zhang, Y., 2014. Chem. Soc. Rev. 43, 506-517.

Liu, L. Z., Song, C., Zhang, Z., Yang, J., Zhou, L. L., Zhang, X., Xie, G. M., 2015. Biosens. Bioelectron. 70, 351-357.

Lin, M. H., Wen, Y. L., Li, L. Y., Pei, H., Liu, G., Song, H. Y., Zuo, X. L., Fan, C. H., Huang, Q., 2014. Anal. Chem. 86, 2285-2288.

Lu, Z., Liu, M., Stribinskis, V., Klinge, C. M., Ramos, K. S., Colburn, N. H., Li, Y., 2008. Oncogene. 27, 4373-4379.

Medina, P. P., Slack, F. J., 2008. Cell. Cycle. 7, 2485-2492.

Pei, H., Lu, N., Wen, Y. L., Song, S. P., Liu, Y., Yan, H., Fan, C. H., 2010. Adv. Mater. 22, 4754-4758.

Radisavljevic, B., Radenovic, A., Brivio J., Giacometti, V., Kis, A., 2011. Nat. Nanotechnol. 6, 147-150

Sawyers, C. L., 2008. Nature. 452, 548-552.

Shuai, H. L., Huang, K. J., Zhang, W. J., Cao, X. Y., Jia, M. P., 2017. Sens. Actuators B-Chem. 243, 403-411.

Su, S., Sun, H. F., Cao, W. F., Chao, J., Peng, H., Zuo, X. L., Yuwen, L. H., Fan, C. H., Wang, L. H., 2016. ACS Appl. Mater. Interfaces. 8, 6826-6833.

Su, S., Sun, H. F., Xu, F., Yuwen, L. H., Wang, L. H., 2013. Electroanalysis. 25, 2523-2529.

Su, S., Wu, Y., Zhu, D., Chao, J., Liu, X. F., Wan, Y., Su, Y., Zuo, X. L., Fan, C. H., Wang, L. H., 2016. Small. 12, 3794-3801.

Su, S., Zhang, C., Yuwen, L. H., Chao, J., Zuo, X. L., Liu, X. F., Song, C. Y., Fan, C. H., Wang, L. H., 2014. ACS Appl. Mater. Interfaces. 6, 18735-18741.

Su, S., Zou, M., Zhao, H., Yuan, C. F., Xu, Y. A., Zhang, C., Wang, L. H., Fan, C. H., Wang, L. H., 2015. Nanoscale. 7, 19129-19135.

Tang, L. H., Wang, Y., Liu, Y., Li, J. H., 2011. ACS Nano. 5, 3817-3822.

Thavanathan, J., Huang, N. M., Thong, K. L., 2014. Biosens. Bioelectron. 55, 91-98.

Tian, Y., Wang, Y., Xu, Y., Liu, Y., Li, D., Fan, C. H., 2015. Sci. China. Chem. 58, 514-518.

Wang, T. Y., Zhu, H. C., Zhuo, J. Q., Zhu, Z. W., Papakonstantinou, P., Lubarsky, G., Lin, J., Li, M. X., 2013. Anal. Chem. 85, 10289-10295.

Wang, T. Y., Zhu, R. Z., Zhuo, J. Q., Zhu, Z. W., Shao, Y. H., Li, M. X., 2014. Anal. Chem. 86, 12064-12069.

Wang, X., Chu, C. C., Shen, L., Deng, W. P., Yan, M., Ge, S. G., Yu, J. H., Song, X. R., 2015. Sens. Actuators B-Chem. 206, 30-36.

Wen, Y. L., Pei, H., Shen, Y., Xi, J. J., Lin, M. H., Lu, N., Shen, X. Z., Li, J., Fan, C. H., 2012. Sci.

Rep. 2, 867.

Wu, X. Y., Chai, Y. Q., Yuan, R., Zhuo, Y., Chen, Y., 2014. Sens. Actuators B-Chem. 203, 296-302.

Yang, H., Hui, A., Pampalakis, G., Soleymani, L., Liu, F. F., Sargent, E. H., Kelley, S. O., 2009. Angew. Chem. Int. Ed. 48, 8461-8464.

Zhang, G. J., Chua, J. H., Chee, R. E., Agarwal, A., Wong, S. M., 2009. Biosens. Bioelectron. 24, 2504-2508.

Zhang, J., Song, S. P., Wang, L. H., Pan, D., Fan, C. H., 2007. Nat. Protoc. 2, 2888-2895.

Zhang, S. S., Xia, J. P., Li, X. M., 2008. Anal. Chem. 80, 8382-8388.

Zhu, C. F., Zeng, Z. Y., Li, H., Li, F., Fan, C. H., Zhang, H., 2013. J. Am. Chem. Soc. 135, 5998-6001.

Scheme 1. Schematic of label-free and dual-mode electrochemical assay for microRNA-21 detection based on gold nanoparticle-decorated MoS_2 nanosheet.

Figure 1. TEM images of (A) MoS_2 nanosheet and (B) AuNPs@MoS_2 nanocomposite. Inset: the statistical diameter of AuNPs on the surface of MoS_2 nanosheet.

Figure 2. (A) Cyclic voltammograms of (a) AuNPs@MoS_2/GCE, (b) DNA1/AuNPs@MoS_2/GCE, (c) MCH/DNA1/AuNPs@MoS_2/GCE, (d) DNA2-AuNPs@MoS_2/MCH/DNA1/AuNPs@MoS_2/GCE and (e) DNA2-AuNPs@MoS_2/miRNA-21/MCH/DNA1/AuNPs@MoS_2/GCE in 10 mM Tris buffer (pH 7.4) with 100 mM $[Ru(NH_3)_6]^{3+}$ and 100 mM KNO_3. Scan rate: 100 mV/s. (B) Nyquist plots of (a) bare GCE, (b) MoS_2/GCE, (c) AuNPs@MoS_2/GCE, (d) DNA1/AuNPs@MoS_2/GCE, (e) MCH/DNA1/AuNPs@MoS_2/GCE, (f) DNA2-AuNPs@MoS_2/MCH/DNA1/AuNPs@MoS_2/GCE and (g) DNA2-AuNPs@MoS_2/miRNA-21/MCH/DNA1/AuNPs@MoS_2/GCE in 10 mM Tris buffer (pH 7.4) containing 5 mM $K_3[Fe(CN)_6]$, 5 mM $K_4[Fe(CN)_6]$ and 0.1 M KCl.

Figure 3. (A) DPV curves and (B) the corresponding calibration curves of MoS_2-based biosensor incubated with different concentration of miRNA-21 (from a to g: 0, 10 fM, 100 fM, 1 pM, 10 pM, 100 pM, 1 nM) in 10 mM Tris–HCl buffer (pH 7.4) with 100 mM $[Ru(NH_3)_6]^{3+}$ and 100 mM KNO_3,. (C) EIS curves and (D) the corresponding calibration curve of MoS_2-based biosensor incubated

with different concentration of miRNA-21 in 10 mM Tris–HCl containing 5 mM $K_3[Fe(CN)_6]$, 5 mM $K_4[Fe(CN)_6]$ and 0.1 M KCl (pH 7.4).

Figure 4. (A) DPV responses of DNA2/MCH/DNA1/AuNPs@MoS_2/GCE (a) before and (b) after the addition of 1 nM miRNA-21, (B) DPV responses of DNA2-AuNPs@MoS_2/MCH/DNA1/AuNPs@MoS_2/GCE (a) before and (b) after the addition of 1 nM miRNA-21 in 10 mM Tris–HCl buffer (pH 7.4) with 100 mM $[Ru(NH_3)_6]^{3+}$ and 100 mM KNO_3. (C) EIS responses of DNA2/MCH/DNA1/AuNPs@MoS_2/GCE (a) before and (b) after the addition of 1 nM miRNA-21, (D) EIS responses of DNA2-AuNPs@MoS_2/MCH/DNA1/AuNPs@MoS_2/GCE (a) before and (b) after the addition of 1 nM miRNA-21 in 10 mM Tris–HCl containing 5 mM $K_3[Fe(CN)_6]$, 5 mM $K_4[Fe(CN)_6]$ and 0.1 M KCl (pH 7.4).

Figure 5. Comparison of (A) DPV and (B) EIS measurements in the presence of miRNA-21, SM-miRNA-21 and miRNA-486, respectively. The concentrations of miRNA-21, SM-miRNA-21 and miRNA-486 were all 100 pM.

Highlights

- A dual-mode electronic biosensor is developed for microRNA-21 (miRNA-21) detection based on gold nanoparticle-decorated MoS_2 nanosheet (AuNPs@MoS_2).
- Both DPV and EIS measurements are used to detect miRNA-21 in ideal buffer and real samples with high sensitivity and selectivity.
- It is important to choose suitable detection methods for nanomaterials-based electrochemical biosensors according to the properties of different nanomaterials, which could maximize the detection signal.

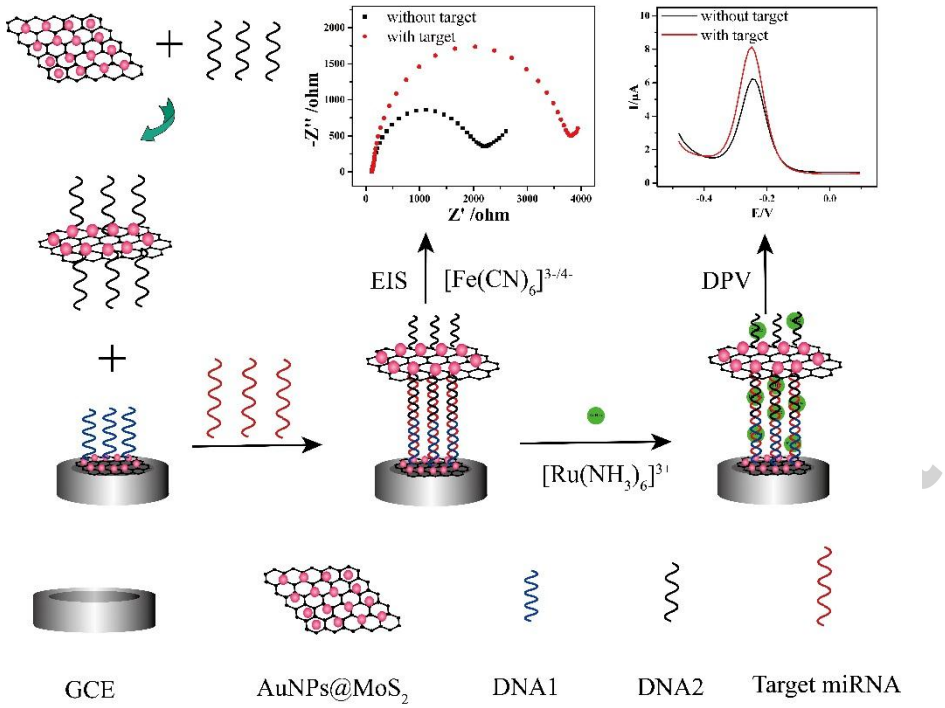

Scheme 1 Su *et al.*

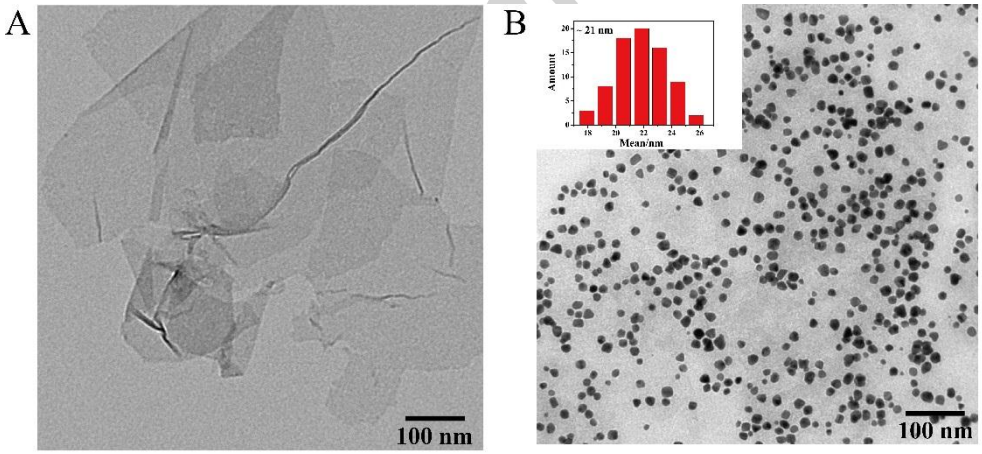

Figure 1 Su *et al.*

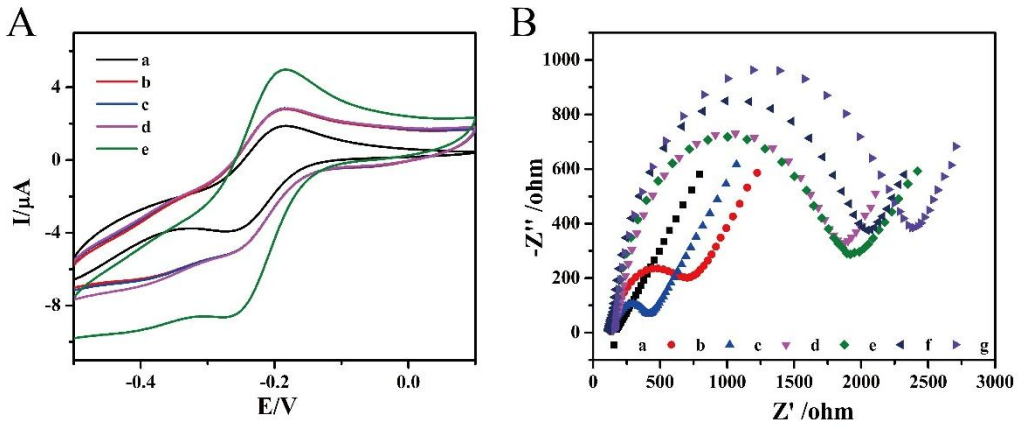

Figure 2 Su *et al.*

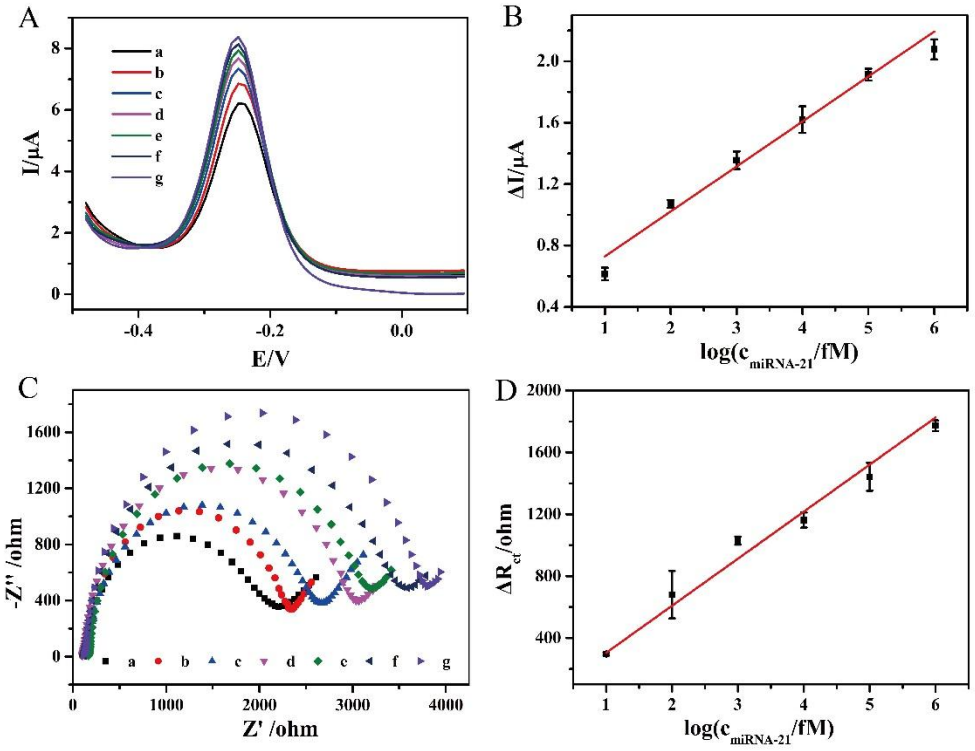

Figure 3 Su *et al.*

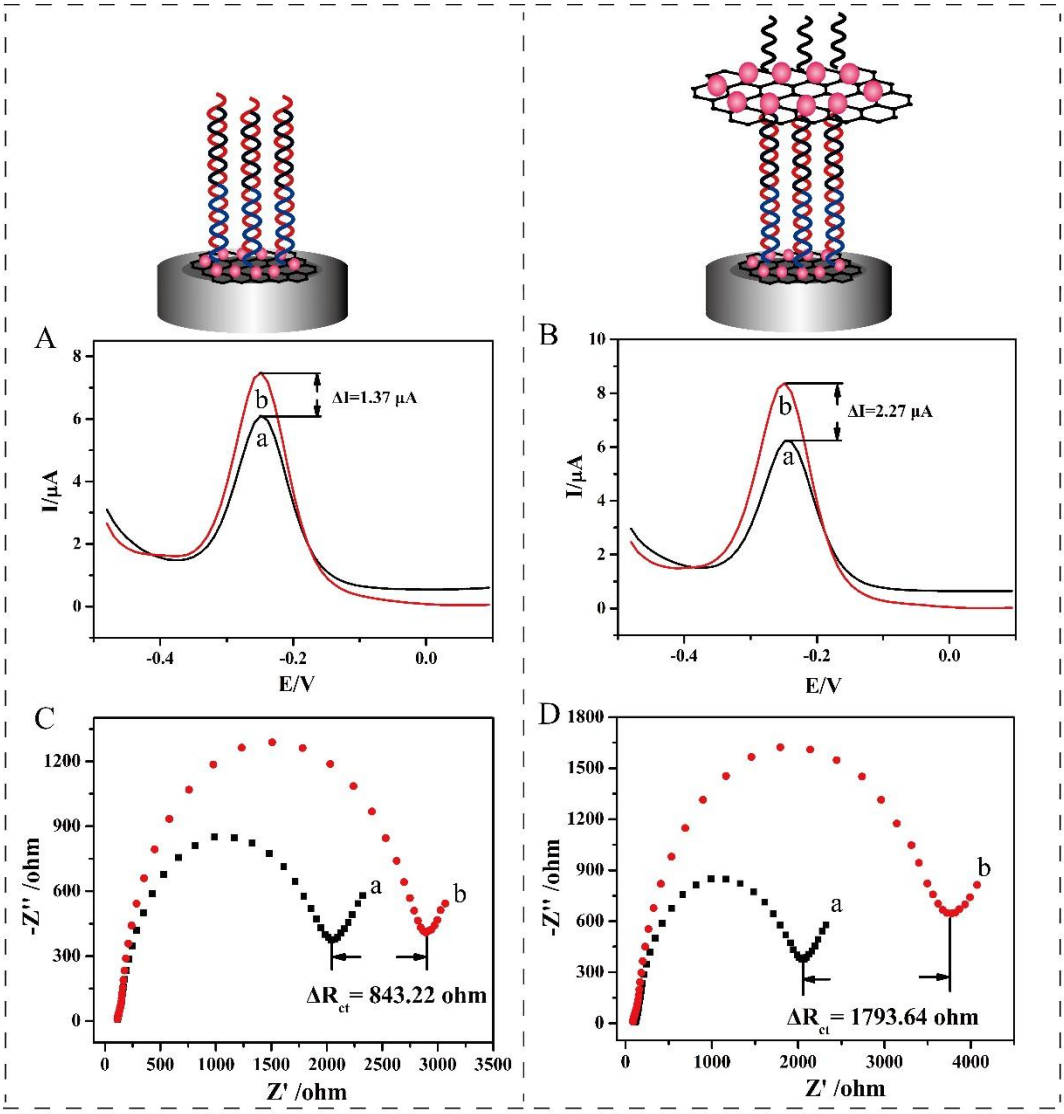

Figure 4 Su *et al.*

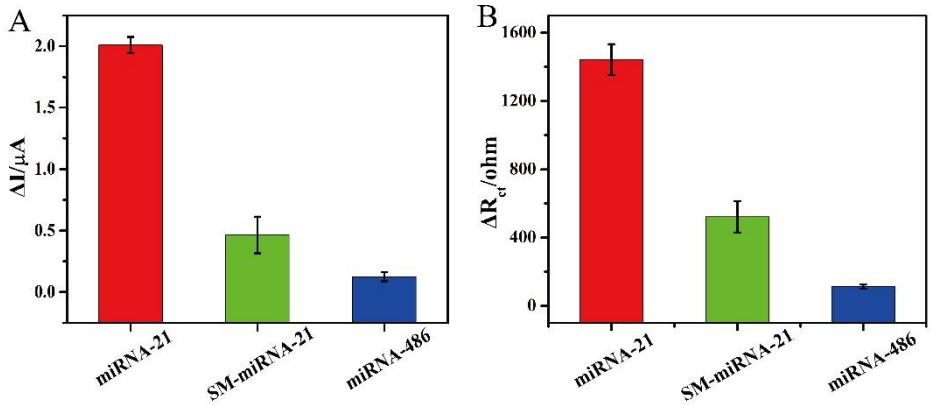

Figure 5 Su *et al.*